Muonic helium atom as a classical three-body problem

T. J. Stuchi,[1,*] A. C. B. Antunes,[1] and M. A. Andreu[2,†]
[1]*Instituto de Física, Universidade Federal do Rio de Janeiro, Caixa Postal 68.528, 21945-970 Rio de Janeiro, RJ, Brazil*
[2]*Departmento de Matemàtica Aplicada i Anàlisi, Universidad de Barcelona, Gran Via 585, 08007–Barcelona, Spain*
(Received 15 December 1999)

We study the classical problem of the muonic helium atom, a helium atom with one of its electrons replaced by a muon. First, we establish the connection of the model with the one-dimensional frozen planetary approximation of the helium atom and find that there is classically stable motion for the configuration α-particle–electron–muon, and no stable motion for the α-particle–muon–electron configuration. After that, we introduce the restricted muonic helium problem, a model for the movement of an electron in the potential of the α particle/muon pair moving in a circular orbit. In this model, the equilibrium points, their associated Lyapunov families of periodic orbits, and their stability parameters were studied. The most interesting feature is the stability of the halo orbits, for a range of energy values. The vicinity of the α particle is also studied, examining Poincaré sections for increasing energy values showing an increase of the chaotic motion.

PACS number(s): 05.45.−a, 31.10.+z

I. INTRODUCTION

Interest in the formation of hadronic atoms goes back to the 1960s when experimental data from helium bubble chambers showed at-rest decay of pions and kaons [1,2]. The experimental data of Iwasaki *et al.* [3] show an instance of kaons bound to He^+. Yamazaki *et al.* [4] observed $\bar{p}$-atom formation. This experiment seems to corroborate the trapping hypothesis formulated by Condo [5] to justify the experiments of the early 1960s. Richter *et al.* [6] suggest a new state of antiprotons bound to atoms with a highly polarized electron located between the nucleus and the antiproton. These states were inspired by classical considerations of two electrons in the field of a point nucleus in which both electrons are on the same side of the nucleus (''planetary'' atoms). We search for such states (see below in Sec. III).

Although helium and heliumlike atoms are essentially quantum systems, a classical approach to these systems might hint at different binding possibilities. Characteristics of these systems that can be obtained by classical methods are the equilibrium points. The determination of these points and their stability might be used to predict the local probability distribution given by quantization. Phenomena typically quantic, like interferences, cannot be analyzed by classical methods. Thus, effects of exchange forces cannot be considered in this framework.

The helium atom has been the object of several classical analyses. Some authors considered the possible equilibrium configurations of the system [7,8]. These configurations are shown to be collinear. Other authors used a purely numerical approach to determine the orbits of the system for several kinds of dynamical configuration [9]. Heliumlike systems have also been studied using a numerical approach [10,11] and several dynamical configurations were examined by these authors. In this paper we deal with a muonic helium atom in which one electron is replaced by a muon.

In Sec. III we analyze the one- and two-dimensional cases. The known stable motion for the unidimensional helium atom [7,8] also exists for our case if we take the configuration α-particle–electron–muon. This agrees with the findings of [6] for the antiproton. There is no unidimensional stable orbit if we consider the configuration α-particle–muon–electron. However, in a rotating system of reference, the analysis of the forces present in this system permits the conclusion that there is only one possible collinear equilibrium configuration, which is a center-center-saddle configuration.

The preliminary estimates shown in Sec. IV encourage the derivation of the restricted muonic problem. The gravitational restricted three-body problem (RTBP) has been widely studied by many authors (see, for instance, [12,13]). In a similar way, in Sec. IV we derive a model with the muon in circular orbit around the α particle in a synodical reference system. This is called the restricted muonic helium problem (RMHP). This model has three equilibrium points. Its linear stability and the zero velocity curves (ZVC) are discussed in Sec. V.

In Sec. VI we calculate the Lyapunov periodic orbits associated with the equilibrium points. As in the gravitational case there is a bifurcation where halo orbits are produced. The interesting feature is that these can be stable for a certain range of energy values. This provides stable orbits where the electron moves, energetically speaking, outside the α-particle well, while the muon orbits the α particle in a circular orbit. According to Kolmogorov-Arnol'd-Moser (KAM) theory there is a two-parameter Cantorian set of three-dimensional (3D) invariant tori around each stable halo orbit.

In Sec. VII we regularize the electron–α-particle collision and present some numerical results, showing that the retrograde orbits are more stable than the direct ones. In fact, there are retrograde KAM tori subsisting for energy values higher than that of the saddle-center point. These orbits, the halo orbits, and their surrounding 3D tori are instances of regular stable orbits outside the energy boundary of the

*Email address: tstuchi@if.ufrj.br
†Email address: mangel@maia.ub.es

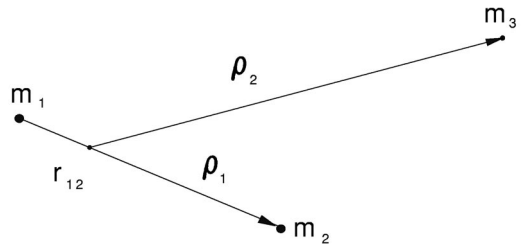

FIG. 1. Jacobi's coordinates for three masses.

α-particle particle well. In this sense they are related to the unidimensional approximation or frozen planetary approximation (FPA).

II. THE FULL PROBLEM IN AN INERTIAL FRAME

Consider three particles P_i, $i=1,2,3$, with masses m_i at positions given by $\boldsymbol{r}_i$, with respect to an inertial Cartesian frame (x,y,z) with origin at the center of mass of the system. In this frame we define Jacobi's coordinates as follows:

$$\boldsymbol{\rho}_1=\boldsymbol{r}_2-\boldsymbol{r}_1, \quad \boldsymbol{\rho}_2=\boldsymbol{r}_3-\boldsymbol{r}_{12}, \quad \boldsymbol{r}_{12}=\frac{m_1\boldsymbol{r}_1+m_2\boldsymbol{r}_2}{m_1+m_2}, \tag{1}$$

where $\boldsymbol{r}_{12}$ gives the position of the center of mass of the particles P_1 and P_2 (see Fig. 1).

The kinetic energy $T=\frac{1}{2}\Sigma_j m_j\dot{\boldsymbol{r}}_j$ expressed in Jacobi's coordinates is given by:

$$T=\frac{1}{2}\mu_{12}\dot{\boldsymbol{\rho}}_1^2+\frac{1}{2}\mu_3\dot{\boldsymbol{\rho}}_2^2, \tag{2}$$

where the reduced masses are $\mu_{12}=m_1m_2/m_1+m_2$ and $\mu_3=m_3(m_1+m_2)/(m_1+m_2+m_3)$. The conjugate momenta to $\boldsymbol{\rho}_1$ and $\boldsymbol{\rho}_2$ are $\boldsymbol{p}_1=\mu_{12}\dot{\boldsymbol{\rho}}_1$ and $\boldsymbol{p}_2=\mu_3\dot{\boldsymbol{\rho}}_2$, respectively. For the potential energy we have

$$V(\boldsymbol{\rho}_1,\boldsymbol{\rho}_2)=V_{12}(\boldsymbol{\rho}_1)+V_{13}\left(\boldsymbol{\rho}_2+\frac{m_2}{m_1+m_2}\boldsymbol{\rho}_1\right)+V_{23}\left(\boldsymbol{\rho}_2-\frac{m_1}{m_1+m_2}\boldsymbol{\rho}_1\right), \tag{3}$$

so that the energy of the system is $H(\boldsymbol{\rho}_1,\boldsymbol{\rho}_2,\boldsymbol{p}_1,\boldsymbol{p}_2)=T+V$.

Now we take P_1, P_2, and P_3 as α particles, muons, and electrons with charges $Q_1=2e$ and $Q_2=Q_3=-e$, so that we have the classical configuration of a heliumlike atom. The values of the masses used are $m_\alpha=m_1=4.002\,602$ u, $m_\mu=m_2=0.110\,303\,035$ u, $m_e=m_3=(5.485\,799\times10^{-4}$ u and u$=931.494\,32$ Mev$/c^2$, where u is the unit of atomic mass.

The only forces acting on the particles are their mutual Coulomb attraction or repulsion. This is the main dynamical difference from the gravitational three-body problem, where the forces depend only on the masses and are always attractive. In our case, we will neglect the gravitational forces since they are much smaller than the Coulomb ones.

We then have that the general form of the Hamiltonian is

$$H(\boldsymbol{\rho}_1,\boldsymbol{\rho}_2,\boldsymbol{p}_1,\boldsymbol{p}_2)=\frac{\boldsymbol{p}_1^2}{2\mu_{12}}+\frac{\boldsymbol{p}_2^2}{2\mu_3}+e^2\left[-\frac{2}{|\boldsymbol{\rho}_1|}-\frac{2}{|\boldsymbol{\rho}_2+[m_2/(m_1+m_2)]\boldsymbol{\rho}_1|}+\frac{1}{|\boldsymbol{\rho}_2-[m_1/(m_1+m_2)\boldsymbol{\rho}_1|}\right]. \tag{4}$$

The associated Hamiltonian equations are

$$\dot{\boldsymbol{p}}_i=-\frac{\partial H}{\partial\boldsymbol{\rho}_i}, \quad \dot{\boldsymbol{\rho}}_i=\frac{\partial H}{\partial\boldsymbol{p}_i} \quad \text{for} \quad i=1,2. \tag{5}$$

This system has six degrees of freedom and its phase space has dimension 12 since we have already used the integrals of the center of mass. The only constants of motion left are now the Hamiltonian itself and the angular momentum, which reduces the phase space dimension to 8, a four-degrees-of-freedom problem. We start dealing with the planar case to gain some insight into its dynamical properties. Throughout this paper all quantities shown in the figures are dimensionless.

III. PLANAR MOTION

We take ϕ and ψ as the angles made by $\boldsymbol{\rho}_1$ and $\boldsymbol{\rho}_2$ with the x direction, respectively, and $\hat{\boldsymbol{\rho}}_1,\hat{\boldsymbol{\phi}},\hat{\boldsymbol{\rho}}_2,\hat{\boldsymbol{\psi}}$ is the associated orthonormal basis. The momenta can be written as

$$p_1=\mu_{12}\dot{\rho}_1, \quad p_\phi=\mu_{12}\rho_1^2\dot{\phi}, \quad p_2=\mu_3\dot{\rho}_2, \quad p_\psi=\mu_3\rho_2^2\dot{\psi}, \tag{6}$$

so that the kinetic energy is

$$T(\rho_1,\phi,\rho_2,\psi,p_1,p_\phi,p_2,p_\psi)=\frac{1}{2\mu_{12}}\left(p_1^2+\frac{p_\phi^2}{\rho_1^2}\right)+\frac{1}{2\mu_3}\left(p_2^2+\frac{p_\psi^2}{\rho_2^2}\right). \tag{7}$$

The potential energy expressed in terms of $\theta=\psi-\phi$ becomes

$$V(\rho_1,\rho_2,\theta)=e^2\left\{-\frac{2}{\rho_1}-2\left[\rho_2^2+\left(\frac{m_2\rho_1}{m_1+m_2}\right)^2+\frac{2m_2}{m_1+m_2}\rho_1\rho_2\cos\theta\right]^{-1/2}+\left[\rho_2^2+\left(\frac{m_1\rho_1}{m_1+m_2}\right)^2-\frac{2m_1}{m_1+m_2}\rho_1\rho_2\cos\theta\right]^{-1/2}\right\} \tag{7a}$$

and the constants of motion are obviously $H=T+V$ and the angular momentum $L=\mu_{12}\rho_1^2\dot{\phi}+\mu_3\rho_2^2\dot{\psi}$.

A. The unidimensional problem

First, we study the possibility of existence of stable unidimensional configurations, that is, $L=\dot{\phi}=\dot{\psi}=0$. The electron and muon are moving unidimensionally and the problem is reduced to two degrees of freedom. In the case of the helium atom, for initial conditions α-particle–electron–

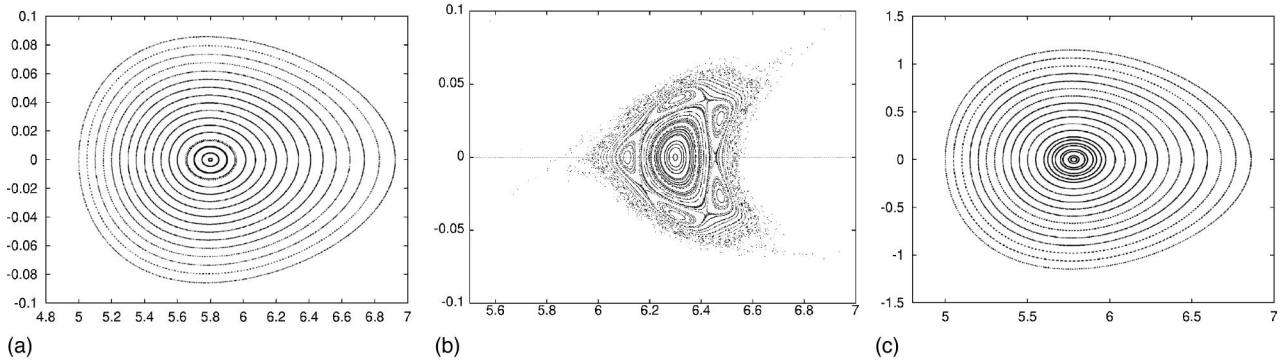

FIG. 2. Poincaré section (ρ_2, p_2), $E=-1$, $\rho_1=0$, and $p_1>0$ for the one-dimensional atom (a) α-e-e; (b) α-m_2-e, $m_2/m_e=30$; (c) α-e-μ.

electron, there exists stable motion for this situation known as the frozen planetary approximation (see [6–8]). We investigate the possibility of such an approximation for muonic helium.

The Hamiltonian can be obtained from Eq. (4) and it is

$$H(\rho_1,\rho_2,p_1,p_2)=\frac{p_1^2}{2\mu_{12}}+\frac{p_2^2}{2\mu_3}+e^2\left[-\frac{2}{|\rho_1|}-\frac{2}{|\rho_2+[m_2/(m_1+m_2)]\rho_1|}+\frac{1}{|\rho_2-[m_1/(m_1+m_2)\rho_1|}\right]. \quad (8)$$

The collision of the α particle and muon has been regularized in the way explained in Sec. VII below. Different values of the mass m_2 have been considered, from the mass of the electron m_e to the mass of the muon m_μ. For each value of the mass m_2, integrating the regularized Hamiltonian equations, Poincaré sections for $\{\rho_1=0,\ p_1>0\}$ have been computed. Figure 2(b) shows one of these sections for the particle with $m_2/m_e=30$; the periodic orbit that corresponds to the FPA is at 6.3, and it bifurcates to an unstable orbit around $m_2/m_e=35$. Therefore the system α-particle—muon–electron, $m_2/m_3>200$, does not have this unidimensional stable configuration.

However, if we regularize the electron–α-particle collision and continue the problem from the electron equilibrium point at 5.8, changing the mass of m_2 as above, the equilibrium remains up to $m_2/m_e=m_\mu/m_e=201.070\,132$. This agrees with the findings of [6] for the antiproton. The Poincaré section of the helium case and of muonic helium are show in Fig. 2(a) and 2(c). Note that the equilibrium point in Fig. 2(c) is only slightly shifted to the left. However, the orbits around the equilibrium point are much slower in the muon case. Samples of typical muon and electron orbits near the resonant one are shown in Figs. 3(a) and 3(b), respectively.

B. Circular orbits

Since we have seen that there is no stability for the configuration α-μ-e in an inertial reference frame, we are going to investigate if there are collinear equilibria with respect to a rotating frame with angular velocity ω, that is, with circular orbits for the three particles in an inertial frame of reference.

We now search for collinear equilibria, and for such we set $\theta=0$, $\psi=\phi$, or $\theta=\pi$, $\psi=\phi+\pi$. In this case $\omega=\dot{\phi}=\dot{\psi}$ is the common angular frequency. From the conservation of angular momentum we have $L/\omega=\mu_{12}\rho_1^2+\mu_3\rho_2^2$, and can take $\rho_2^2=(1/\mu_3)(L/\omega-\mu_{12}\rho_1^2)$ to express both ρ_2 and $\dot{\rho}_2$ in terms of ρ_1 and $\dot{\rho}_1$ in the Hamiltonian given by Eqs. (7) and (7a). The new Hamiltonian for the collinear motion is

$$H=\frac{\omega L}{2}+\frac{1}{2\mu_{12}}\left[1+\frac{\mu_{12}}{\mu_3}\left(\frac{\rho_1}{\rho_2}\right)^2\right]p_1^2+V_\pm(\rho_1) \quad (9)$$

with

$$V_\pm(\rho_1)=Q^2\left[-\frac{2}{\rho_1}-2\left|\rho_2\pm\frac{m_2}{m_1+m_2}\rho_1\right|^{-1}+\left|\rho_2\mp\frac{m_1}{m_1+m_2}\rho_1\right|^{-1}\right], \quad (10)$$

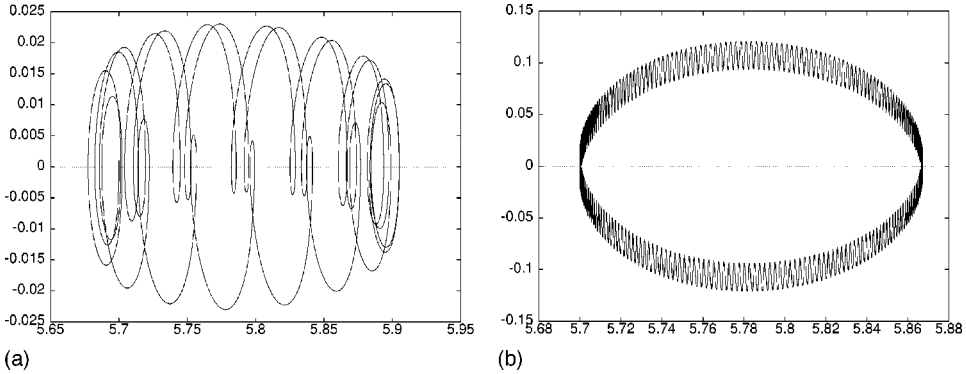

FIG. 3. Typical orbits (ρ_2, p_2) near the equilibrium configurations: (a) electron orbit in case of Fig. 2(a); (b) muon orbit in case of Fig. 2(c).

where ρ_2 takes the value mentioned above, and the indices $\pm$ stand for $\cos\theta = \pm 1$.

The singularities of the potential are $\rho_1 = 0$ and

$$\rho_1^j = \left[\frac{L}{\omega\mu_3} \left(\frac{\mu_{12}}{\mu_3} + \frac{m_j^2}{(m_1+m_2)^2} \right)^{-1} \right]^{1/2},$$

where $j = 1,2$. If $\rho_1 = 0$, we have the maximum value of ρ_2, $\rho_{2max} = \sqrt{L/\omega\mu_3}$, and conversely, if $\rho_2 = 0$, then $\rho_{1max} = \sqrt{L/\omega\mu_{12}}$.

For the case of a muon there is only one equilibrium point, found for V_-, i.e., when $\theta = \pi$. Its value is $\rho_{1e} = 0.940\,037\,73$ which corresponds to $\rho_{2e} = 4.771\,376\,98$ in units of ρ_{1max}. At this point the second derivative of the potential is negative, a maximum, which means an unstable fixed point.

The equilibrium position of the electron, ρ_{2e}, being reasonably far away from the pair α-particle–muon allows us to look at the problem of an electron moving in the potential created by the pair revolving about their common center of mass. Of course, this approximation becomes better for motions of the electron around and near this position. However, numerical tests show that the approximation is acceptable under less stringent requirements. In the next section we study the reduction to a restricted three-body Coulomb problem in synodic coordinates. We claim that findings with such an approximation can be used to get information on the full system by continuation reasoning.

IV. THE RESTRICTED MUONIC HELIUM PROBLEM

Suppose that the α and muon particles are moving in circular orbits around their center of mass. We are going to derive the equations of motion of an electron under the Coulomb forces of the α-particle–muon pair. This restricted muonic helium problem approximation of the full problem has to be handled with care. On the other hand, the full problem may be written as a RMHP plus perturbations. That would allow us to obtain orbits of the full problem by means of continuation techniques.

Moreover, in this approximation, we essentially assume that the motion of the electron does not disturb the uniform circular motion of the muon around the helium nucleus. A sufficient condition for the validity of this assumption is that the distance of the electron from the α particle is much larger than the α-particle–muon distance. The sufficiency of this condition can be evaluated by comparing the position of the equilibrium point given by the exact solution in Sec. III and the approximate calculation of the next section. The relative error is 0.004 564 8.

Another circumstance in which the approximate description may be used is in some cases of a very rapid passage of the electron near the α particle. It can be shown that, if the time of interaction is sufficiently small, the impulse transmitted by the electron to the muon may be neglected.

We considered very elongated orbits of the electron along the negative x axis, turning around the α particle in the rotating frame. The recoil velocity of the muon in the x direction ($v_{\mu x}$), due to the electron impulse, is compared with the muon velocity in the circular orbit of the inertial frame ($v_{\mu c}$). The relation $v_{\mu x}/v_{\mu c}$ is energy dependent, as can be seen in the table below.

$-E$	36	38	40	70	100
$v_{\mu x}/v_{\mu c}$	0.11	0.049	0.030	0.013	0.001

By inspection, we see that for energies lower than $E = -40.0$ the impulse of the electron on the muon becomes negligible. These calculations were done using the regularization described in Sec. VII. We proceed now to present the RMHP.

To derive the equations of the RMHP we find first the parameters of the circular motion of the muon around the α particle. This is a two-body problem. Consider an inertial reference frame with the origin at the center of mass. Let $\boldsymbol{r}_1$ and $\boldsymbol{r}_2$ by the vector positions of the masses m_1 and m_2, which are the masses of the α and muon particles, respectively. The relative position is denoted by $\boldsymbol{\rho} = \boldsymbol{r}_2 - \boldsymbol{r}_1$. We also have

$$\boldsymbol{r}_1 = \frac{-\mu}{m_1}\boldsymbol{\rho}, \quad \boldsymbol{r}_2 = \frac{\mu}{m_2}\boldsymbol{\rho},$$

where the mass parameter is $\mu = m_1 m_2/(m_1+m_2)$. The charges of the α and muon particles are $Q_1 = 2e$ and $Q_2 = -e$, respectively. Defining as ϕ the angle of $\boldsymbol{\rho}$ with the x direction, the energy of the system can be written as

$$E = \frac{1}{2}\mu(\dot{\rho}^2 + \rho^2\dot{\phi}^2) - \frac{2e^2}{\rho}. \tag{11}$$

Taking into account the conservation of the angular momentum of the system, $L = \mu\rho^2\dot{\phi}$, and the minimum of the corresponding effective potential, the radius of the circular orbit ρ_{cir}, and its corresponding angular velocity are

$$\rho_{cir} = \frac{L^2}{2\mu e^2}, \quad \omega = \frac{4\mu e^4}{L^3}.$$

So they satisfy the relationship

$$\omega^2\rho_{cir}^3 = \frac{2e^2}{\mu}, \tag{12}$$

similar to Kepler's third law.

We now take a frame centered at the center of mass, rotating with the constant angular velocity ω and with the x axis having the direction of ρ. Here, the mass of the electron is denoted by m and its position is $\boldsymbol{r}$. In this system the equation of motion for the electron is

$$m\frac{d^2\boldsymbol{r}}{dt^2} = \boldsymbol{F}_1 + \boldsymbol{F}_2 - m\boldsymbol{\omega}\times(\boldsymbol{\omega}\times r) - 2m\boldsymbol{\omega}\times\frac{d\boldsymbol{r}}{dt}, \tag{13}$$

where $\boldsymbol{\omega} = \omega\hat{\mathbf{z}}$ and the Coulomb forces of the α particle and the muon on the electron are given by

$$\boldsymbol{F}_1 = -2e^2\frac{\boldsymbol{r}-\boldsymbol{r}_1}{|\boldsymbol{r}-\boldsymbol{r}_1|^3}, \quad \boldsymbol{F}_2 = e^2\frac{\boldsymbol{r}-\boldsymbol{r}_2}{|\boldsymbol{r}-\boldsymbol{r}_2|^3}, \tag{14}$$

where $\boldsymbol{r}_1=x_1\hat{\mathbf{x}}$, $\boldsymbol{r}_2=x_2\hat{\mathbf{x}}$ with $x_1=-(\mu/m_1)\rho_{cir}$ and $x_2=(\mu/m_2)\rho_{cir}$. Expressing Eq. (13) in Cartesian rotating coordinates, we get

$$\begin{aligned}
\ddot{x}&=-\frac{e^2}{2m}\left[\frac{2(x-x_1)}{r_1^3}-\frac{x-x_2}{r_2^3}\right]+\omega^2 x+2\omega\dot{y},\\
\ddot{y}&=-\frac{e^2}{2m}\left[\frac{2}{r_1^3}-\frac{1}{r_2^3}\right]y+\omega^2 y-2\omega\dot{x},\\
\ddot{z}&=-\frac{e^2}{2m}\left[\frac{2}{r_1^3}-\frac{1}{r_2^3}\right]z,
\end{aligned}\tag{15}$$

where $r_i^2=(x-x_i)^2+y^2+z^2$, for $i=1,2$. To use a dimensional coordinates we perform the change

$$X_1=x_1/\rho_{cir},\quad X_2=x_2/\rho_{cir},$$

$$\boldsymbol{R}=\boldsymbol{r}/\rho_{cir},\quad \tau=\omega t.$$

Denoting the variables with lower case letters again, we have the following set of equations:

$$\begin{aligned}
\ddot{x}-2\dot{y}&=\frac{\partial V}{\partial x}=-\frac{\overline{\mu}}{2}\left[\frac{2(x-x_1)}{r_1^3}-\frac{x-x_2}{r_2^3}\right]+x,\\
\ddot{y}+2\dot{x}&=\frac{\partial V}{\partial y}=\left[1-\frac{\overline{\mu}}{2}\left(\frac{2}{r_1^3}-\frac{1}{r_2^3}\right)\right]y,\\
\ddot{z}&=\frac{\partial V}{\partial z}=-\frac{\overline{\mu}}{2}\left[\frac{2}{r_1^3}-\frac{1}{r_2^3}\right]z,
\end{aligned}\tag{16}$$

where the derivatives are now with respect to the a dimensional time τ. Moreover, we have introduced the parameter $\overline{\mu}=\mu/m=195.677\,717\,5$, for the present values. We note that the relationship (12) was used in the derivation of Eqs. (16). The potential function is then defined as

$$V(x,y,z)=\frac{\overline{\mu}}{2}\left[\frac{2}{r_1}-\frac{1}{r_2}\right]+\frac{1}{2}(x^2+y^2).\tag{17}$$

This system has an integral of motion similar to the Jacobi integral for the RTBP:

$$C_J=2V-(\dot{x}^2+\dot{y}^2+\dot{z}^2),\tag{18}$$

C_J being the Jacobi constant of motion. Therefore, we can write a Hamiltonian for the system,

$$H(\boldsymbol{q},\boldsymbol{p})=\frac{1}{2}(p_x^2+p_y^2+p_z^2)+yp_x-xp_y-\overline{\mu}\left[\frac{1}{r_1}-\frac{1}{2r_2}\right],\tag{19}$$

with $\boldsymbol{q}=(x,y,z)$ and $\boldsymbol{p}=(p_x,p_y,p_z)$. The conjugate momenta are expressed by $p_x=\dot{x}-y$, $p_y=\dot{y}+x$, and $p_z=\dot{z}$, and therefore the Coriolis potential appears rather than the centrifugal potential. We note that the value of the Hamiltonian function is $-C_J/2$.

The corresponding Hamilton equations can easily be derived and they are

$$\begin{aligned}
\dot{x}&=p_x+y,\\
\dot{y}&=p_y-x,\\
\dot{z}&=p_z,\\
\dot{p}_x&=p_y-\overline{\mu}\left[\frac{x-x_1}{r_1^3}-\frac{x-x_2}{2r_2^3}\right],\\
\dot{p}_y&=-p_x-\overline{\mu}\left[\frac{1}{r_1^3}-\frac{1}{2r_2^3}\right]y,\\
\dot{p}_z&=-\overline{\mu}\left[\frac{1}{r_1^3}-\frac{1}{2r_2^3}\right]z.
\end{aligned}\tag{20}$$

These equations present two symmetries:

$$S_1:(x,y,z,\dot{x},\dot{y},\dot{z},t)\leftrightarrow(x,y,-z,\dot{x},\dot{y},-\dot{z},t),\tag{21}$$

$$S_2:(x,y,z,\dot{x},\dot{y},\dot{z},t)\leftrightarrow(x,-y,z,-\dot{x},\dot{y},-\dot{z},-t).\tag{22}$$

The equations of the RTBP also present the same symmetries S_1 and S_2. They are useful for looking for periodic orbits.

V. FIXED POINTS AND THEIR LINEAR STABILITY

We can find the fixed points of system (16) by taking $V_x=V_y=V_z=0$, i.e., setting the partial derivatives of the potential-like function equal to zero, as well as $\dot{x}=\dot{y}=\dot{z}=0$, or, equivalently, as the equilibrium positions of the Hamiltonian vector field. Both lead to the following set of equations for the configuration variables:

$$x-\frac{\overline{\mu}(x-x_1)}{r_1^3}+\frac{\overline{\mu}(x-x_2)}{2r_2^3}=0,\tag{23}$$

$$\left(1-\overline{\mu}\left[\frac{1}{r_1^3}-\frac{1}{2r_2^3}\right]\right)y=0,\tag{24}$$

$$-\overline{\mu}\left[\frac{2}{r_1^3}-\frac{1}{r_2^3}\right]z=0.\tag{25}$$

First, we look for collinear equilibrium points, that is, with $y=z=0$. Later on, we will see that there are also two additional equilibrium points with $z\neq 0$.

Then, in the collinear case, the previous system is reduced to Eq. (23). One can look for an equilibrium point on the left of the α particle, between it and the muon, or on the right of the muon particle. Each case leads to a quintic equation that has to be solved numerically. It is easy to see that only the first case is possible. To look for solutions on the negative axis to the left of the α particle, we call $\xi=r_1=x_1-x$; then $r_2=x_2-x=1+\xi$ and $x=x_1-\xi$. Equation (23) becomes

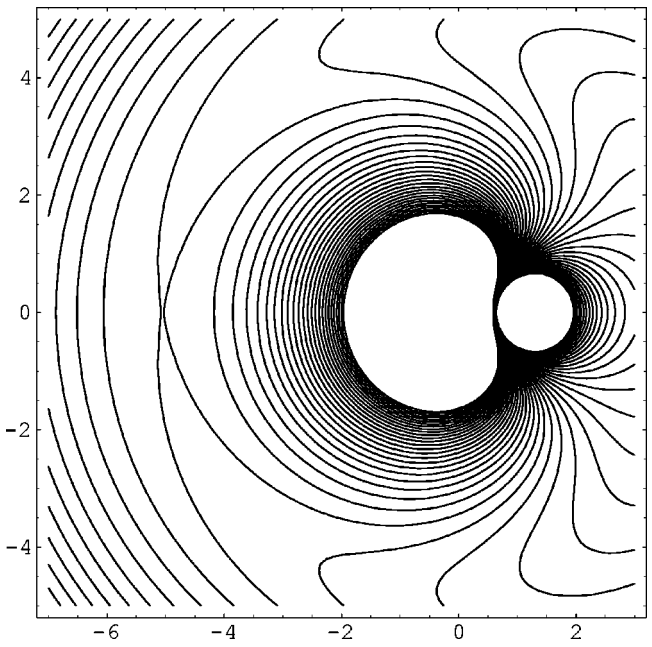

FIG. 4. The zero velocity curves of the RMHP. The inner closed curves on the left allow bounded motion around the α particle; the right hand closed curves are the repulsive barrier of the muon.

$$\xi - x_1 - \frac{\overline{\mu}}{\xi^2} + \frac{\overline{\mu}}{2(1+\xi)^2} = 0, \tag{26}$$

and we obtain the quintic equation

$$2\xi^5 + 2(2-x_1)\xi^4 + 2(1-2x_1)\xi^3 - (2x_1 + \overline{\mu})\xi^2 - 4\overline{\mu}\xi - 2\overline{\mu} = 0. \tag{27}$$

Using $x_1 = -0.026\,818\,770$, $x_2 = 0.973\,181\,23$, and $\overline{\mu} = 195.677\,717\,5$, the positive solution of Eq. (27) gives the equilibrium point at $x_0 = -5.052\,559\,73$. Note that this solution is quite close to the value we found in the full problem (see Sec. III B).

Figure 4 shows the zero velocity curves of the RMHP. In this figure, the saddle-center character (on the x-y plane) of the equilibrium point is visible. The energy of the equilibrium point is $h_0 = -35.462\,460\,13$. For lower values of the energy the Hill regions are bounded around the α particle. Conversely, for values of the energy higher than h_0 the Hill regions are unbounded.

We shall now examine the linear approximation in the neighborhood of the equilibrium point. The linearization of Eqs. (20) around the equilibrium point is

$$\begin{pmatrix} \dot{\eta}_1 \\ \dot{\eta}_2 \\ \dot{\eta}_3 \\ \dot{\eta}_4 \\ \dot{\eta}_5 \\ \dot{\eta}_6 \end{pmatrix} = \begin{pmatrix} 0 & 1 & 0 & 1 & 0 & 0 \\ -1 & 0 & 0 & 0 & 1 & 0 \\ 0 & 0 & 0 & 0 & 0 & 1 \\ 2a & 0 & 0 & 0 & 1 & 0 \\ 0 & -a & 0 & -1 & 0 & 0 \\ 0 & 0 & -a & 0 & 0 & 0 \end{pmatrix} \begin{pmatrix} \eta_1 \\ \eta_2 \\ \eta_3 \\ \eta_4 \\ \eta_5 \\ \eta_6 \end{pmatrix}, \tag{28}$$

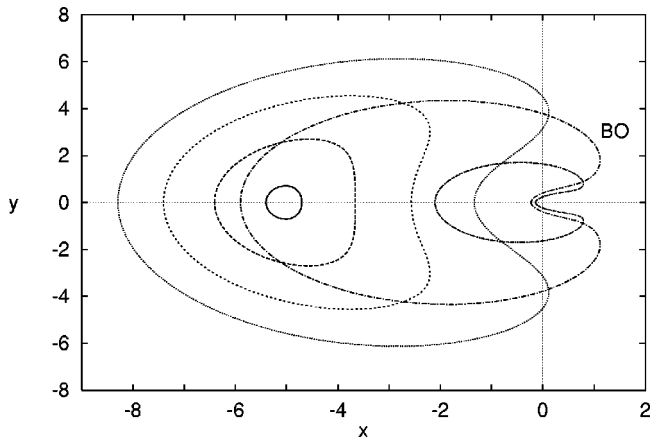

FIG. 5. The family of planar Lyapunov periodic orbits. The orbit labeled as BO is the bifurcating orbit from which halo orbits appear.

where

$$a = \frac{\overline{\mu}}{(x_1 - x_0)^3} - \frac{\overline{\mu}}{(x_2 - x_0)^3}.$$

The eigenvalues of this system are $\pm 1.078\,905\,96i$, $\pm 0.508\,283\,18$ and $\pm 1.046\,094\,51i$, showing that the equilibrium point is a center-saddle-center point. We also want to comment that by performing a linear symplectic change of variables $\eta = S\zeta$ it is possible to express the Hamiltonian of the system (28) as

$$H_2 = \frac{1.078\,905\,96}{2}(\zeta_1^2 + \zeta_2^2) + 0.508\,283\,18\zeta_3\zeta_4 + \frac{1.046\,094\,51}{2}(\zeta_5^2 + \zeta_6^2). \tag{29}$$

Moreover, the Eqs. (23), (24), and (25) have a pair of solutions with $z \neq 0$. They are $(3.291\,470\,90, 0, \pm 2.054\,586\,76)$. We note that this kind of equilibrium point does not appear in the gravitational RTBP. In this case, the eigenvalues of the linearization of Eq. (20) are $\pm 0.962\,566\,456\,i$, $\pm 0.849\,046\,032 \pm 0.919\,283\,615\,i$.

VI. LYAPUNOV AND HALO ORBITS

In the previous section, the linear stability of the equilibrium points was discussed. The knowledge of periodic orbits is important for some semiclassical methods and leads to promising results [7,14–17]. We now present the periodic orbits around those points. In the collinear case, the Hamiltonian system (20) has two families of periodic orbits emanating from the equilibrium point. Each family corresponds to one of the harmonic oscillators of the linearized system (28). These families of orbits are usually called Lyapunov orbits [18].

The problem of finding a periodic orbit is reduced to looking for a fixed point of the Poincaré map defined by the flow of Eq. (20) through a transverse section. In our case, we have used the section $\{y = 0\}$. Figure 5 shows several orbits of the planar Lyapunov family. We notice that as Lyapunov orbits

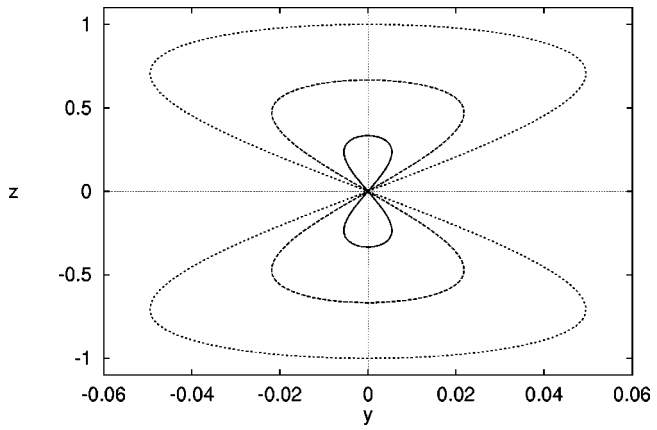

FIG. 6. y,z projection of the vertical Lyapunov orbits that, as in the RTBP, are 8 shaped. Notice that these orbits are very narrow in the y direction.

grow and approach collision they move to the right. A continuation method (also called the homotopy method) has been used to follow the periodic orbits along the family (for more details about the numerical methods see [19,20]).

To study the linear stability of each orbit, its monodromy matrix has been used. The monodromy matrix is obtained by integrating the variational equations along the orbit. Because of the Hamiltonian character of the system, the (eventually complex) eigenvalues of the monodromy matrix are of the form λ_1, $1/\lambda_1$, λ_2, $1/\lambda_2$, apart from 1, with multiplicity 2. The stability parameters are defined as $s_k=\lambda_k+1/\lambda_k$ for $k=1,2$. An orbit is linearly stable if its stability parameters are real and their absolute values are less than 2.

The planar Lyapunov orbits near the equilibrium point are elliptic-hyperbolic. The hyperbolic directions are on the x-y plane, while the elliptic one corresponds to the z coordinate. The bifurcation of the halo occurs when there is a change from stable to unstable in the Lyapunov family in the z direction. In Fig. 5 the bifurcating orbit has been labeled as BO.

Figure 6 shows several orbits of the vertical Lyapunov family of periodic orbits. They are called vertical because they start from the equilibrium point in the direction of the z coordinate and they are very narrow in the x and y directions. Sometimes they are also called the 8-shaped family. As far as we have followed this family, all the orbits are elliptic-hyperbolic.

Another way to understand why the bifurcation of the halo orbits takes place as follows. We recall that we saw in Sec. V that the equilibrium point has two different frequencies, but they are quite close. Following the family of planar Lyapunov orbits, the frequency (or the period, if you prefer) varies. Moreover, the frequency in the vertical direction also varies along this family. The bifurcation of the Halo occurs when the frequency of the Lyapunov orbit coincides with the frequency in the vertical direction. There, two families of

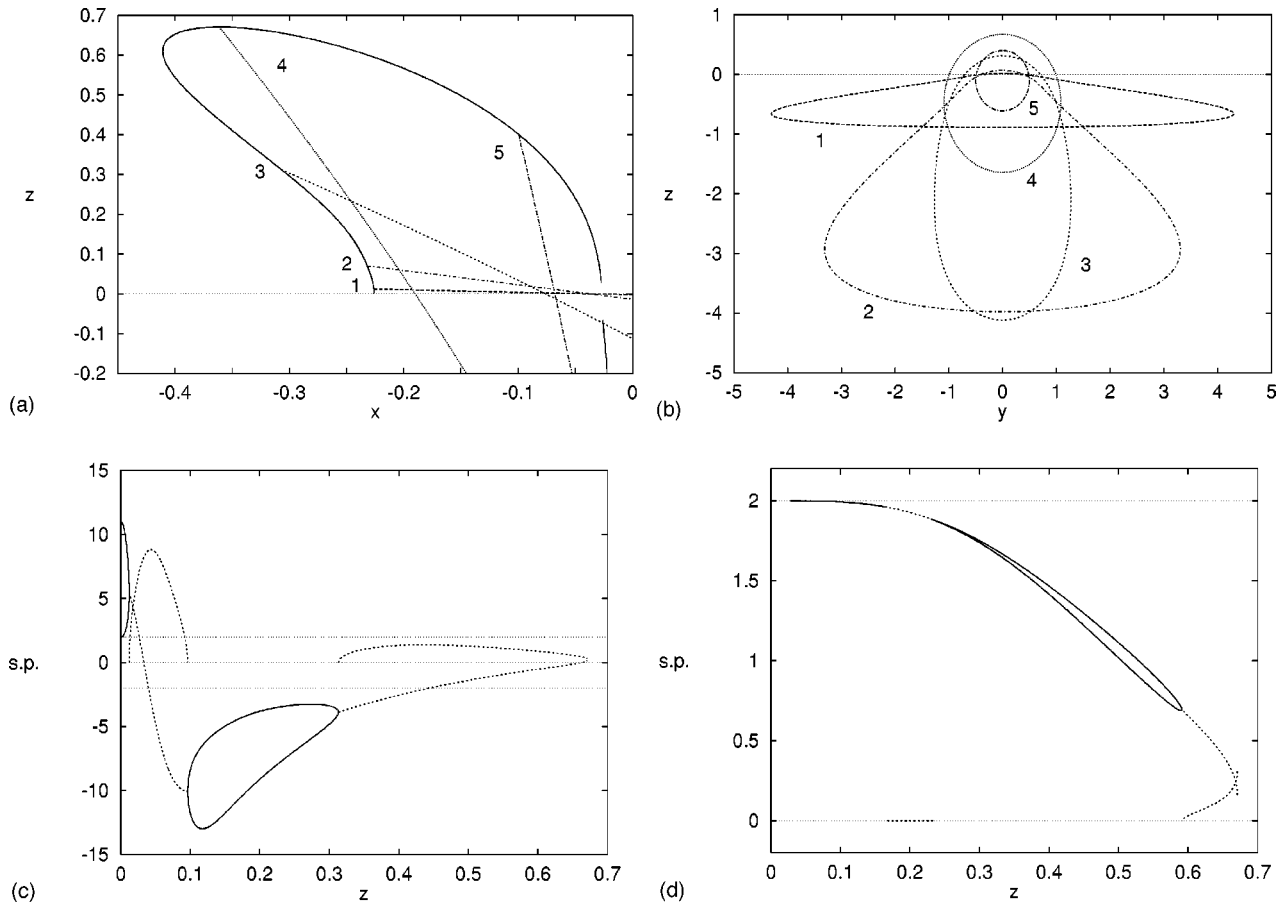

FIG. 7. (a) Detail of the evolution of the halo orbits in the x,z projection; (b) the y,z projection; (c) evolution of the stability parameters from the bifurcation up to the orbit with maximum z; (d) continuation of the stability parameters from z maximum toward the α particle. The orbits $z\in(0.233,0.591)$ and $z<0.16$ are all stable.

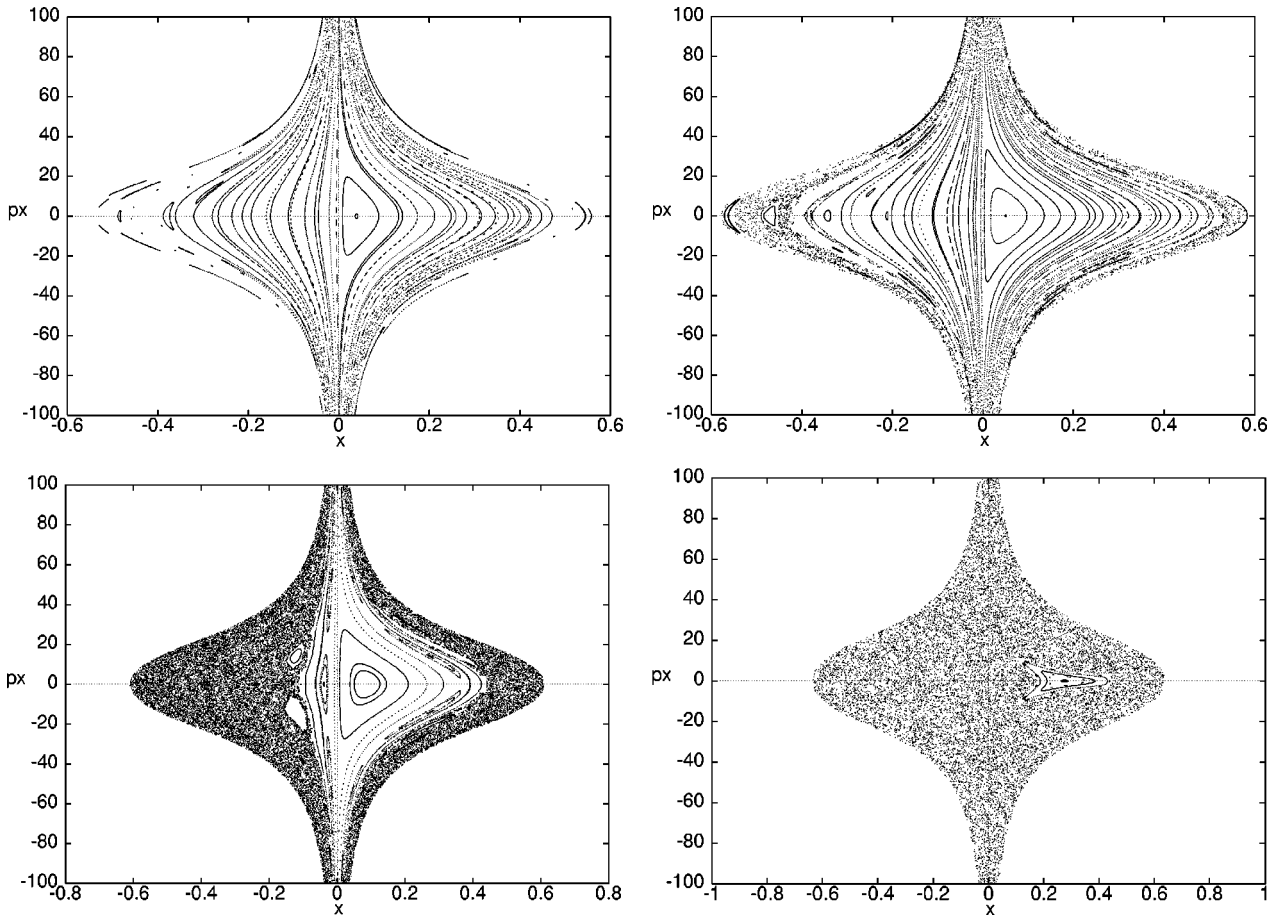

FIG. 8. Left to right, top to bottom: Poincaré section $y=0, p_y<0$ in physical variables for $-E=120.0$, 100.0, 70.0, and 38.0. The right hand side represents retrograde orbits while the left hand side shows direct orbits of the electron.

halo orbits are created. These families are symmetric with respect to the x-y plane because of the symmetry (21).

Figure 7(a) shows a detail of evolution of the one of the halo families (x,z projection). The solid line shows the maximum and minimum values of z reached by them. Figure 7(b) shows the y,z projection of some of these orbits. The evolution of the stability parameter from the bifurcation up to the maximum z value reached by the halo orbits is shown in Fig. 7(c). The continuous line represents real stability parameters s_1 and s_2. In regions where they are complex conjugate we show the real and imaginary parts of s_1 with a discontinuous line. After the z-maximum orbit we still continue the family toward the α particle. This evolution is shown in Fig. 7(d). It is very important to point out that for $z\in(0.233,0.591)$ the orbits are stable. They are also stable for $z<0.16$, but they are small orbits rather near the α particle.

Stable halo orbits have two normal frequencies, besides the proper frequency. According to KAM theory [21,22], around each halo orbit there is a two-parameter Cantorian family of 3D invariant tori. This family of tori can be labeled with three parameters: one for the corresponding periodic halo orbit and two more for the amplitudes with respect to that halo orbit. The frequency, generically, varies on moving these parameters. The family of 3D invariant tori is not a continuous family, it is a Cantor set, and there are gaps between the tori. An electron orbiting in one of these gaps may escape as a consequence of Arnol'd's diffusion [23]. However, the time to escape would certainly be very long [24]. So there is a subset of the phase space around stable halo orbits where an electron may probably remain for a long time. Sometimes, such subsets are said to be effectively stable. We also want to comment that the 3D invariant tori can be computed using the numerical method described in [25] or semianalytically using the Lindstedt-Poincaré method as in [26]. But this computation is beyond the scope of this article.

Finally, we want to comment that we have also computed the Lyapunov families of periodic orbits emanating from the equilibrium points with $z\neq 0$. All those orbits have some (real or complex) unstable part and so they are not interesting unless the quantization method is such as to need summation over all periodic orbits [16].

VII. REGULARIZATION OF THE ELECTRON–α-PARTICLE COLLISION

To study numerically the bounded orbits in the vicinity of the α particle, it is convenient to regularize the electron–α-particle collision. The singularity of the muon does not affect numerical calculations since it is a repulsive singularity.

In the planar case, i.e., for two degrees of freedom, this is easily done through the Levi-Civitá procedure. However, the three-degrees-of-freedom case is much more involved since in this case the extension of the Levi-Civitá procedure re-

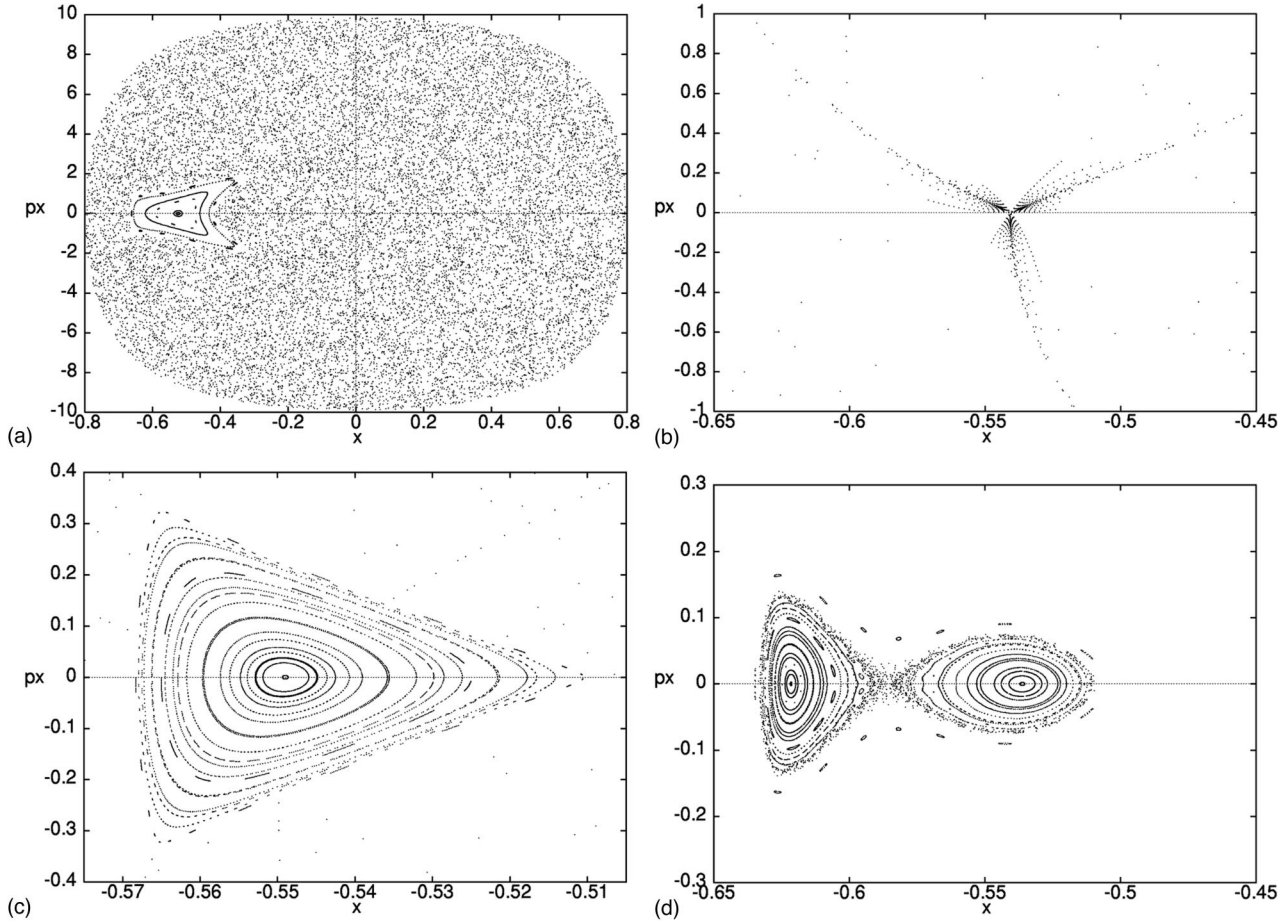

FIG. 9. Display of retrograde KAM remnant curves in Levi-Civitá variables. (a) $E=-38.0$; (b) $E=-37.0$ (note that the triangular KAM tori structure collapses to an unstable orbit); (c) $E=-36.5$ (the triangular structure reappears inverted); (d) $E=-34.5$.

quires a four-degrees-of-freedom configuration with one constraint. In that case, it is necessary to use the Kustaanheimo-Stiefel transformation [27,28]. Here, we shall deal only with the planar case.

We make a translation to bring the α particle to the origin, $\overline{x}=x-x_1$, so that Hamiltonian (19) becomes (calling $\overline{x}$, x again)

$$\overline{H}=\frac{1}{2}(p_x^2+p_y^2)+yp_x-(x+x_1)p_y + \overline{\mu}\left[\frac{1}{(x^2+y^2)^{1/2}}-\frac{1}{2((x-1)^2+y^2)^{1/2}}\right]. \tag{30}$$

We now apply the change of variables known as the Levi-Civitá transformation, given by

$$\begin{pmatrix} x \\ y \end{pmatrix}=\begin{pmatrix} \hat{x} & -\hat{y} \\ \hat{y} & \hat{x} \end{pmatrix}\begin{pmatrix} \hat{x} \\ \hat{y} \end{pmatrix}, \tag{31}$$

the induced conjugate momenta transformation being

$$\begin{pmatrix} p_x \\ p_y \end{pmatrix}=\frac{2}{\hat{r}^2}\begin{pmatrix} \hat{x} & -\hat{y} \\ \hat{y} & \hat{x} \end{pmatrix}\begin{pmatrix} \hat{p}_x \\ \hat{p}_y \end{pmatrix}, \tag{32}$$

where $\hat{r}^2=(\hat{x}^2+\hat{y}^2)=r=(x^2+y^2)^{1/2}$. To complete the regularizing procedure it is also necessary to change the time scale,

$$d\hat{\tau}=\frac{4\ d\tau}{r}. \tag{33}$$

Using Eqs. (31), (32), and (33) in $\hat{H}(\hat{\mathbf{q}},\hat{\mathbf{p}})=(r/4)[\overline{H}(\hat{\mathbf{q}},\hat{\mathbf{p}})+p_0]$, the regularized Hamiltonian is (suppressing carets)

$$H=\frac{p_0}{2}\frac{(x^2+y^2)}{2}+\frac{1}{2}(p_x^2+p_y^2)+\frac{1}{2}(x^2+y^2)(yp_x-xp_y) - \frac{x_1(yp_x+xp_y)}{2}+\frac{\overline{\mu}(x^2+y^2)}{8[(x^2+y^2)^2-2(x^2-y^2)+1]^{1/2}}, \tag{34}$$

with $c=p_0/2=-\overline{h}/2$, where $\overline{h}$ is the chosen value of the energy branch of $\overline{H}$.

Numerical results

As expected, integration of the equations derived from the Hamiltonian (34) allows comfortable numerical work. The first thing we point out is the fact that the chaotic region is

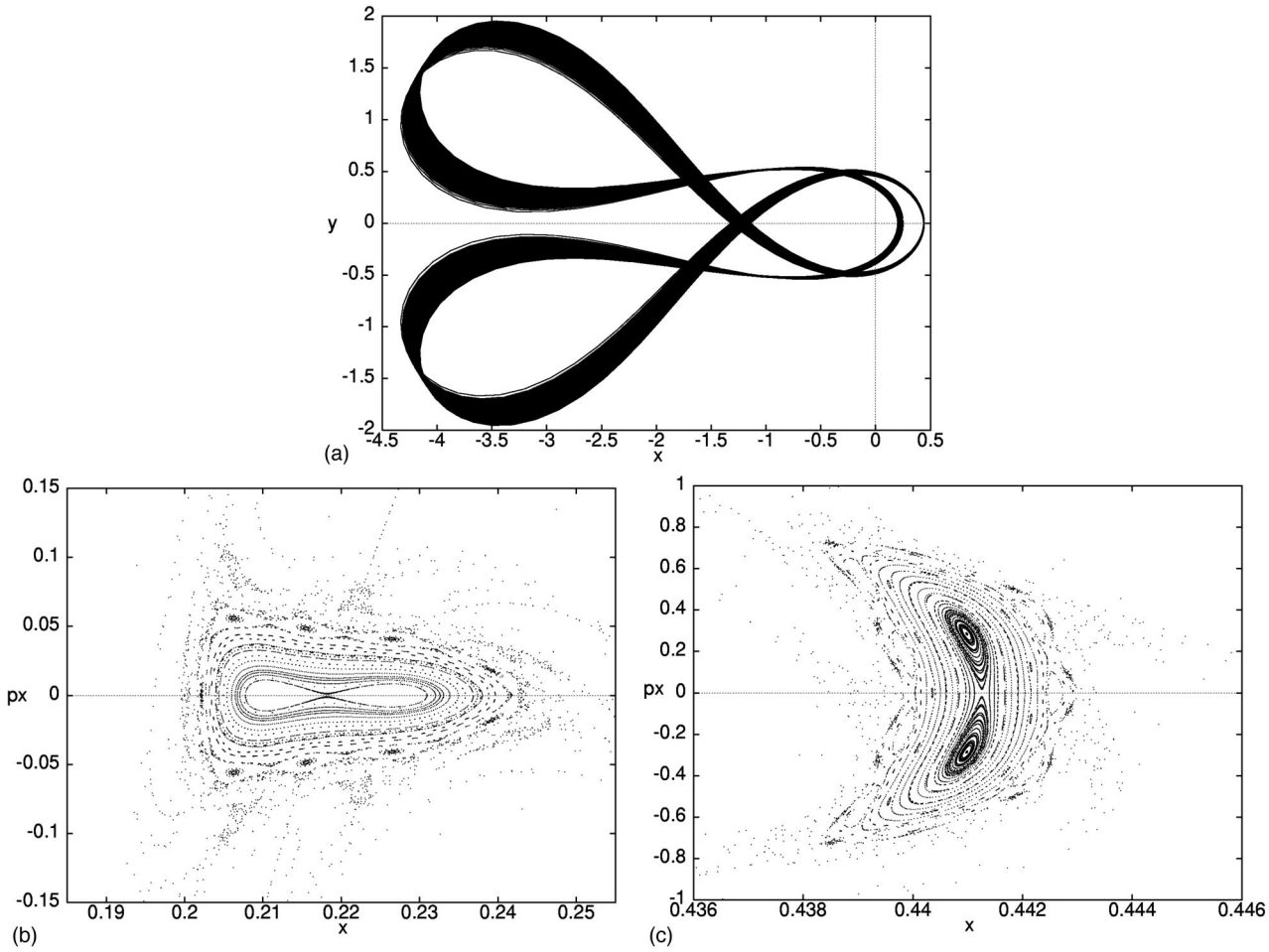

FIG. 10. The small KAM zone for $E=-33.8$ when the fixed points in the Poincaré map of Fig. 9(d) have bifurcated: (a) orbit in the configuration space; (c) and (d) details of the Poincaré section in physical variables.

fairly large even for values of the energy far from the open ZVC. We show in the next figures the Poincaré section defined by $y=0$, $\dot{y}<0$. The initial conditions were chosen in the physical variables just before the regularizing transformation with the α particle at the origin. This is cumbersome but it helps to keep track of the original physical problem.

In Fig. 8 we show some Poincaré sections in physical variables. These are obtained from the section in Levi-Civitá variables by applying the inverse transformation. To be able to show the sections of retrograde and direct motion in the same figure we changed the sign of the x variable for the direct orbits and they are shown on the left hand side of the figure. The sections for the direct orbits show that they become completely chaotic before the retrograde ones. The retrograde orbits, on the left of the figure, stay on KAM tori for a certain range of energy higher than the energy of the saddle center, i.e, after the opening of the ZVC. This is shown in Fig. 9 in Levi-Civitá variables. Before the ZVC open, the triangular shaped KAM region is inverted [Fig. 9(c)], after collapsing [Fig. 9(b)], and subsists after the ZVC open. In Fig. 10(a) we show a projection onto the configuration space of this final KAM region for $E=-33.8$ using the physical variables. There is no persistent large KAM region as in the Hill problem [29].The details of the tiny islands of the Poincaré section are shown also in physical variables in Figs. 10(c) and 10(d). As can be seen in these figures, the bound orbits (periodic and tori) always pass between the muon and the α particle.

VIII. FINAL COMMENTS

The full classical problem for muonic helium is a four-degrees-of-freedom problem. The only Hamiltonian systems that are completely understood (classically) are those with two degrees of freedom. So the approximations made in this paper are meant as a contribution toward the understanding of the full problem, with techniques of numerical continuation using the results we present here as first guesses.

The unidimensional atom has proved very useful in the understanding of quantum states in several atoms. The FPA found here for the configuration α-particle–electron–muon suggests the existence of quantum bound states, and these could be confirmed using the Born-Oppenheimer approximation as was done in [6] for antiprotonic helium, since the same arguments used by these authors are also valid for muonic helium.

Our findings near the center-center-saddle equilibrium point on the left of the α-particle–muon pair, in the synodic reference system, are also an interesting feature. The Lyapunov orbits bifurcate into halo orbits that have a range of stability. This means that while the muon revolves around

the α particle in circular motion there are periodic orbits and 3D KAM tori to the left of the pair. There are bound classical states, which might correspond to stable or metastable quantum states since their energy is above the energy of the classical well around the α particle. Since these orbits are surrounded by tori they could be studied with EBK quantization. The same is true for the orbits shown in Fig. 10(a) which also have energy above the limits of the classical well. The difference between these two types of orbit and the FPA is that they always come near or between the central pair, while in the FPA the electron (helium atom) or the heavy particle keeps away from the central pair. Inside the classical well retrograde orbits, i.e., electrons that are slower than the muon in circular orbit, are more regular than faster ones (direct orbits). To conclude, we note again that any periodic orbit of the restricted muonic helium problem can be continued to the orbits of the full problem.

ACKNOWLEDGMENTS

We are very grateful to Alejandro López-Castillo and Carlos Simó for invaluable discussions. M.A.A. wishes to acknowledge the hospitality of the Departmento de Matemàtica Aplicada I, Universitat Politècnica de Catalunya (Barcelona, Spain).

[1] M. M. Block, T. Kikucline, C.R. Seu, and R. Walker, Phys. Rev. Lett. **11**, 301 (1963).
[2] J.G. Petkovich and E.G. Pewitt, Phys. Rev. Lett. **11**, 290 (1963).
[3] M. Iwasaki *et al.*, Phys. Rev. Lett. **67**, 1246 (1991).
[4] T. Yamazaki, M. Aoki, M. Iwasaki, R.S. Hayano, T. Ishikawa, H. Onta, E. Takada, H. Tamura, and A. Sakaguchi, Phys. Rev. Lett. **63**, l590 (1989).
[5] G.T. Condo, Phys. Lett. **9**, 65 (1964).
[6] K. Richter, J.-M. Rost, R. Thurwachter, and J.S. Briggs, Phys. Rev. Lett. **66**, l49 (1991).
[7] A. López-Castillo, M.A.M. de Aguiar, and A.M. Ozorio de Almeida, J. Phys. B **29**, 197 (1996).
[8] D. Wintgen, K. Richter, and G. Tanner, Chaos **2**, 19 (1992).
[9] T. Yamamoto and K. Kaneko, Phys. Rev. Lett. **70**, 1928 (1993).
[10] F. Benvenuto, G. Casati, and D.L. Shepelyansky, Phys. Rev. A **53**, 737 (1996).
[11] E.A. Solov'ev, Zh. Éksp. Teor. Fiz. **89**, 1991 (1985) [Sov. Phys. JETP **62**, 1148 (1986)].
[12] V. Szebehely, *Theory of Orbits* (Academic Press, New York, 1967).
[13] C. Marchal, *The Three-Body Problem* (Elsevier, Amsterdam, 1990).
[14] A. López-Castillo, Phys. Rev. Lett. **77**, 4516 (1996).
[15] A. López-Castillo, Phys. Rev. A **58**, 1846 (1998).
[16] M.C. Gutzviller, *Chaos in Classical and Quantum Mechanics* (Springer, New York, 1990).
[17] A.M. Ozório de Almeida, *Hamiltonian Systems: Chaos and Quantization* (Cambridge University Press, Cambridge, 1988).
[18] C. Siegel and J.K. Moser, *Lectures on Celestial Mechanics* (Springer-Verlag, New York, 1971).
[19] J. Stoer and R. Bulirsch, *Introduction to Numerical Analysis* (Springer-Verlag, Berlin, 1980).
[20] C. Simó, in *Modern Methods in Celestial Mechanics*, edited by D. Benest and C. Froeschlé (Editions Frontières, Paris, 1990).
[21] V.I. Arnol'd, Russ. Math. Survey **18**, 9 (1963).
[22] À. Jorba and J. Villanueva, J. Nonlinear Sci. **7**, 427 (1997).
[23] V.I. Arnol'd, Sov. Math. Dokl. **5**, 581 (1964).
[24] A. Delshams and P. Gutiérrez, J. Diff. Eqns. **128**, 415 (1996).
[25] C. Simó, in *Cent Ans Après les Méthodes Nouvelles de H. Poincaré* (Société Mathématique de France, Paris, 1996), pp. 1–23.
[26] G. Gómez, J. Masdemont, and C. Simó, Astronaut. Sci. (to be published).
[27] E. Stiefel and G. Schiefele, *Linear and Regular Celestial Mechanics* (Springer-Verlag, New York, 1971).
[28] A. Deprit, A. Elipe, and S. Ferrer, Celest. Mech. Dyn. Astron. **58**, 151 (1994).
[29] C. Simó and T.J. Stuchi, Physica D **140**, 1 (2000).